Spatial transcriptomics identifies enriched gene expression and cell types in human liver fibrosis

Brian K. Chung[1,2,3] | Jonas Øgaard[1,2] | Henrik Mikael Reims[4] |
Tom H. Karlsen[1,2,3,5] | Espen Melum[1,2,3,5,6]

[1]Norwegian PSC Research Center, Oslo University Hospital, Rikshospitalet, Oslo, Norway

[2]Research Institute of Internal Medicine, Oslo University Hospital, Rikshospitalet, Oslo, Norway

[3]Institute of Clinical Medicine, Faculty of Medicine, University of Oslo, Oslo, Norway

[4]Department of Pathology, Oslo University Hospital, Rikshospitalet, Oslo, Norway

[5]Section of Gastroenterology, Department of Transplantation Medicine, Division of Surgery, Inflammatory Diseases and Transplantation, Oslo University Hospital, Rikshospitalet, Oslo, Norway

[6]Hybrid Technology Hub-Centre of Excellence, Institute of Basic Medical Sciences, Faculty of Medicine, University of Oslo, Oslo, Norway

Correspondence
Brian K. Chung or Espen Melum, Norwegian PSC Research Center, Division of Surgery, Inflammatory Medicine and Transplantation, Oslo University Hospital Rikshospitalet, Postboks 4950 Nydalen, N-0424 Oslo, Norway.
Email: b.k.chung@medisin.uio.no or espen.melum@medisin.uio.no

Funding information
Helse Sør-Øst RHF, Grant/Award Number: 2015015 and 2018066; Norwegian PSC Research Center; Norges Forskningsråd, Grant/Award Number: 262613 and 325435; PSC Partners Seeking a Cure

Abstract

Liver fibrosis and cirrhosis have limited therapeutic options and represent a serious unmet patient need. Recent use of single-cell RNA sequencing (scRNAseq) has identified enriched cell types infiltrating cirrhotic livers but without defining the microanatomical location of these lineages thoroughly. To assess whether fibrotic liver regions specifically harbor enriched cell types, we explored whether whole-tissue spatial transcriptomics combined with scRNAseq and gene deconvolution analysis could be used to localize cell types in cirrhotic explants of patients with end-stage liver disease (total $n = 8$; primary sclerosing cholangitis, $n = 4$; primary biliary cholangitis, $n = 2$, alcohol-related liver disease, $n = 2$). Spatial transcriptomics clearly identified tissue areas of distinct gene expression that strongly correlated with the total area (Spearman $r = 0.97$, $p = 0.0004$) and precise location (parenchyma, 87.9% mean congruency; range, 73.1%–97.1%; fibrosis, 68.5% mean congruency; range, 41.0%–91.7%) of liver regions classified as parenchymal or fibrotic by conventional histology. Deconvolution and enumeration of parenchymal and fibrotic gene content as measured by spatial transcriptomics into distinct cell states revealed significantly higher frequencies of *ACTA2+ FABP4+* and *COL3A1+* mesenchymal cells, *IL17RA+ S100A8+* and *FCER1G+* tissue monocytes, *VCAM1+ SDC3+* Kupffer cells, *CCL4+ CCL5+ KLRB1+* and *GZMA+ IL17RA+* T cells and *HLA-DR+*, *CD37+ CXCR4+* and *IGHM+ IGHG+* B cells in fibrotic liver regions compared with parenchymal areas of cirrhotic explants. *Conclusion*: Our findings indicate that spatial transcriptomes of parenchymal and fibrotic liver regions express unique gene content within cirrhotic liver and demonstrate proof of concept that spatial transcriptomes combined with additional RNA sequencing methodologies can refine the localization of gene content and cell lineages in the search for antifibrotic targets.

INTRODUCTION

Liver cirrhosis is the end stage of advanced hepatic fibrosis with a growing global disease burden resulting in over 2 million deaths per year.[1] Development of cirrhosis is a gradual process, and fibrosis severity is known to correlate with adverse patient outcomes.[2,3] At present, no clinical approved antifibrotic treatments for liver fibrosis are available except for liver transplantation,[4] and despite major advances in the recent years, the key pathways regulating progression of fibrosis in human liver require additional attention.

Several cell types have been implicated in liver fibrosis using various methodologies, but the molecular and cellular complexity of the hepatic microenvironment remains a key obstacle hindering the development of potential treatments.[5] The advent of single-cell RNA sequencing (scRNAseq) has enabled the identification of specific cellular phenotypes in complex disease,[6] and recent applications of scRNAseq in patients with cirrhosis has uncovered multiple cell types of mesenchymal, endothelial, and monocytic origin increased in end-stage disease.[7,8] Despite these advances, scRNAseq is limited by the necessity of single-cell suspensions that require tissue digestion and homogenization, which prevents the specific localization of gene expression and distinct cells to fibrotic lesions. Traditional technologies determining cellular localization such as immunohistochemistry and *in situ* hybridization are restricted by the use of preselected markers[9] and thus biased *a priori* compared with global and unbiased cellular characterizations of scRNAseq and spatial transcriptomics.[10]

To circumvent the limitations of scRNAseq and traditional methodologies, we performed whole-tissue spatial transcriptomics to assess total gene expression in regions of liver fibrosis. Tissue transcriptomics have been used to identify a shared onco-fetal ecosystem between fetal liver and hepatocellular carcinoma,[11] validate the tissue distribution of hepatocytes, cholangiocytes, and mesenchymal subsets in healthy human liver,[12] and recently applied alongside proteogenomics to localize evolutionarily conserved macrophages in healthy and obese human liver.[13] Herein, we combined tissue transcriptomics with scRNAseq data and gene deconvolution to identify highly enriched gene expression associated with specific cell types localized to parenchymal and fibrotic regions of liver explants from patients with end-stage cirrhosis etiologies that can serve as a foundation for future identification of key pathways in liver fibrosis.

METHODS

Human liver samples, ethics, and consent

End-stage liver biopsies ($n = 8$) from patients with cirrhosis and primary sclerosing cholangitis (PSC; $n = 4$),[14] primary biliary cholangitis (PBC, $n = 2$),[15] or alcohol-related liver disease (ALD, $n = 2$)[16] were collected following liver transplantation (Table 1). Written informed consent was obtained from all study participants, and study ethics were approved by regional Committees for Medical and Health Research Ethics of South East Norway (reference numbers: 2012–286 and 2016–1540) in accordance with the Declaration of Helsinki.

Spatial transcriptomics and sequencing

Cryopreserved 5-mm hilar core biopsies from liver explants were trimmed, embedded in precooled optimal cutting temperature mounting medium (OCT; Tissue-Tek), and quickly refrozen on liquid nitrogen. Two samples per OCT block were combined to maximize coverage of the RNA capture slides (Visium; 10X Genomics). Optimal tissue thickness (10 μm) and time for permeabilization (25 min) were empirically determined using tissue-optimization slides and reagents (10X Genomics). Spatial transcriptomics was then performed as recommend by the manufacturer (User Guide CG000239 Rev D; 10X Genomics). Briefly, tissue was sectioned, positioned onto the RNA capture slides, and left for 5 days at −80°C. Frozen slides were then brought to 37°C for 1 min for equilibration, fixed in methanol, stained 10 s with hematoxylin followed by 1 min in eosin, and rinsed, dried, and digitized without a cover slip using a slide scanner (Axio Scan.Z1; Zeiss). Tissue sections were incubated in permeabilization buffer and then reverse transcription, second strand synthesis and denaturation, complementary DNA (cDNA) amplification, and quality control were performed to ensure proper construction of spatial gene expression libraries (10X Genomics). High-throughput sequencing was performed on a NovaSeq sequencer (Illumina) using a SP 200 cycle flow cell to achieve recommended sequencing depth. Sequencing reads were demultiplexed and aligned to the human genome (GRCh38-2020-A) using Space Ranger (v.1.1.0; 10X Genomics), and spatial transcriptomes were visualized using Loupe Browser software (v.5.0.1; 10X Genomics).

Differential gene analysis

Parenchymal and fibrotic liver regions were first defined using graph-based clustering of total gene content in

TABLE 1 Clinical details of study cohort at time of liver transplantation

Patient ID	Diagnosis	Age (years)	Sex (M/F)	IBD status	UDCA (Y/N)	APRI	FIB-4	MELD-Na	Hb (g/dl)	Platelets (10^9/L)	INR	ASAT (µkat/L)	ALAT (µkat/L)	Albumin (g/dL)	Bilirubin (µmol/L)	Creatinine (µmol/L)	Dialysis (Y/N)
1	PSC	65	F	Crohn	Y	24.1	31.01	38	8.4	36	1.3	5.1	5.2	3.2	916	52	Y
2	PSC	37	M	UC	Y	5.2	8.50	20	11.3	86	1.2	3.3	1.7	3.2	90	71	N
3	PSC	34	M	UC	Y	8.5	8.34	15	13.1	72	1.1	4.6	4.0	3.7	122	63	N
4	PSC	49	M	UC	Y	0.4	0.84	18	8.5	787	1.4	2.4	1.9	2.8	75	68	N
5	PBC/AIH	56	F	–	Y	2.3	4.53	26	8.9	143	2.1	2.0	1.7	2.6	66	90	N
6	PBC	54	F	–	Y	3.5	8.18	20	13.2	90	1.4	1.9	1.1	3.4	208	51	N
7	ALD	53	M	–	N	4.9	13.16	20	13.2	66	1.4	2.4	1.3	3.4	104	80	N
8	ALD	59	M	–	N	0.5	2.93	26	9.5	238	1.6	1.0	0.4	3.4	14	231	Y

Abbreviations: AIH, autoimmune hepatitis; ALAT, alanine aminotransferase; ALD, alcohol-related liver disease; APRI, aspartate aminotransferase to platelet ratio index; ASAT, aspartate transaminase; FIB-4, fibrosis-4 index; Hb, hemoglobin; IBD, inflammatory bowel disease; INR, international normalized ratio; MELD-Na, model for end-stage liver disease sodium; PSC, primary sclerosing cholangitis; PBC, primary biliary cholangitis; UC, ulcerative colitis; UDCA, ursodeoxycholic acid.

Loupe Browser software (10X Genomics). Genes significantly up-regulated or down-regulated between parenchymal and fibrotic regions (log2 fold-change; $p < 0.05$) within the same liver sample were calculated using the "locally distinguishing" feature analysis in Loupe Browser, which filters significant genes using Benjamini-Hochberg correction for multiple testing.

Tissue histopathology and immunofluorescence staining

Scanned tissue sections were used to identify tissue morphological features and pathological changes by an expert liver pathologist (H.M.R.). The main tissue regions of liver parenchyma and fibrosis (portal tracts and connective tissue) were identified by their appearance and the overall tissue architecture after hematoxylin and eosin (HE) staining. HE histological assessment of parenchymal and fibrotic liver regions was confirmed in adjacent sections from the same tissue blocks by Masson's trichrome staining (HT15-1KT; Sigma-Aldrich). Attempts were made to identify bile duct proliferation and inflammation; however, individual cell types, small islands of liver parenchyma, and individual hepatocytes in fibrotic areas could not be definitely identified due to resolution limitations of the histological images. Regions of poor tissue permeability as measured by low total RNA counts and RNA spillover adjacent to tissue (Figure S2) were omitted from spatial transcriptome analysis to minimize tissue heterogeneity within the parenchymal and fibrotic regions during downstream comparisons. For immunofluorescent staining, liver tissue from the same liver blocks used for spatial transcriptomics were sectioned at 10 µm, fixed to Superfrost Plus microscope slides (J1800AMNZ; Thermo Fisher Scientific) at room temperature (RT) and then submerged in 100% methanol for 15 min at −20°C. Slides were washed 3 times in phosphate-buffered saline (PBS) and blocked with 10% goat serum and 1% bovine serum albumin (BSA) in PBS for 1 h at RT. Primary antibody incubations for nicotinamide N-methyltransferase (NNMT; clone OTI3D8; Abcam), collagen type III alpha 1 chain (COL3A1; clone EPR17673; Abcam), actin alpha 2, smooth muscle (ACTA2; clone EPR5368; Abcam), complement C1q C chain (C1QC; clone ab4223; Abcam), CD3D (clone EP4426; Abcam), immunoglobulin heavy constant mu (IGHM; clone PJ2-22H3; Miltenyi Biotec), CD31 (clone JC70A; Dako), CD68 (clone C68/684; Abcam), fatty acid–binding protein 4 (FABP4; clone EPR3579; Abcam), and vascular cell adhesion molecule 1 (VCAM1; clone EPR5047; Abcam) were performed at 1:50 to 1:200 dilutions in 0.1% BSA/PBS overnight at 4°C. Secondary antibody incubations using anti-mouse immunoglobulin G (IgG)-AF488 (clone ab150117; Abcam), anti-mouse IgG-AF568 (clone A-11077; Thermo Fisher Scientific)

or anti-mouse IgG-AF647 (clone A-2124; Thermo Fisher Scientific) were completed for 1 h at RT. Slides were washed 3 times in PBS and cell nuclei were counterstained with Prolong Diamond Antifade mountant with 4′,6-diamidino-2-phenylindole (DAPI; P36962; Thermo Fisher Scientific). Images were taken using a Leica TCS SP8 STED confocal microscope and analyzed by ImageJ 1.53k software (National Institutes of Health). Frequencies and absolute numbers of CD31+ cells represent the normalized mean of CD31+ cells per total cells or CD31+ cells per $100\,\mu m^2$ quantified using QuPath "positive cell detection" analysis of CD31 and DAPI immunofluorescence co-staining in $n = 4$ parenchymal or $n = 4$ fibrotic regions defined by spatial transcriptomics per liver section ($n = 8$).[17]

Gene deconvolution and enumeration of cell fractions by CIBERSORTx

Published scRNAseq data from cirrhotic livers ($n = 66,135$ cells)[7] was randomly down-sampled to 10,000 cells and used to generate CIBERSORTx "signature matrix" files (https://cibersortx.stanford.edu). Signature matrices contained gene profiles of mesenchyme, endothelia, cholangiocytes, plasmacytoid dendritic cells (pDCs), mast cells, monocytes, innate-like lymphocytes (ILCs), B cells, T cells, and cycling cell types and subtypes (Table S1). Next, averaged gene expression (median-normalized) of parenchymal and fibrotic regions were converted into CIBERSORTx "mixture" files containing differential gene expression values measured by spatial transcriptomics (Table S2). The mixture file and the signature matrices were uploaded and run in the "impute cell fractions" module of CIBERSORTx with quantile normalization disabled, permutations set to 100 and batch collection set to S-mode.

Statistical analyses

All values are presented as mean ± SD, and all statistical analysis was performed using Prism 9.2.0 (GraphPad) unless otherwise stated. Correlation between the classification of parenchymal and fibrotic regions by histological and spatial transcriptomics was calculated using two-tailed nonparametric Spearman correlation analysis. For comparative analysis of cell type fractions between parenchymal and fibrotic liver regions, p-values were calculated using parametric two-tailed paired Student's t test. For comparative analysis of cell type fractions between disease groups, p-values were calculated using one-way analysis of variance (ANOVA) followed by Bonferroni's correction for multiple comparison. p-values less than 0.05 were considered significant.

RESULTS

Classification of parenchymal and fibrotic liver regions by spatial transcriptomics

To explore the ability of spatial transcriptomics to discriminative well-defined pathological regions, we first compared the classification of hepatic parenchyma and fibrosis by spatial transcriptomics to conventional histopathology. First, explant tissue from patients with end-stage cirrhosis (total $n = 8$; PSC; $n = 4$; PBC, $n = 2$; ALD, $n = 2$; Table 1) were stained with HE and scanned for histological evaluation (Figure 1A). Next, the exact same tissue sections were permeabilized on RNA capture slides, amplified by polymerase chain reaction (PCR) into cDNA, processed into libraries, and sequenced. Parenchymal and fibrotic histological regions were assessed by an expert hepatopathologist (H.M.R.), while spatial transcriptomes were analyzed by graph-based clustering and topographically positioned onto the scanned HE images (Figure S1). Areas of low RNA yield due to incomplete permeabilization (Figure S2) received an "unassigned" classification and were excluded from downstream transcriptome analysis (Figure 1B). Total numbers of parenchymal and fibrotic liver regions (i.e., RNA capture spots) classified by histology and spatial transcriptomics showed a strong correlation (Spearman $r = 0.97$, $p = 0.0004$; Figure 1C), indicating that areas of distinct histology indeed harbor unique gene profiles that can be consistently distinguished across different samples. Classification of identical RNA capture spots as parenchymal or fibrotic by conventional histology and spatial transcriptomics was also remarkably consistent (parenchyma: 87.9% mean congruency, range: 73.1%−97.1%; fibrosis: 68.5% mean congruency, range: 41.0%−91.7%; Figure 1D), showing that spatial transcriptomes can delineate specific tissue regions within cirrhotic livers and possibly aid the characterization of tissue types when combined with conventional histological assessment. To determine which expressed genes enabled a clear separation between parenchymal and fibrotic regions, we performed targeted differential expression gene analyses of the highly expressed genes (defined as transcripts detected at greater than one read per RNA capture spot) detected by spatial transcriptomics in the parenchymal and fibrotic regions of each liver sample ($n = 8$). We identified a total of $n = 57$ up-regulated genes exclusive to fibrotic liver regions ($p < 0.05$) that corresponded broadly to four biological processes (RNA translation, antigen presentation, fibrogenesis, and immune function), as assessed by STRING protein–protein pathway analysis (Figure 1E and Figure S3).[18]
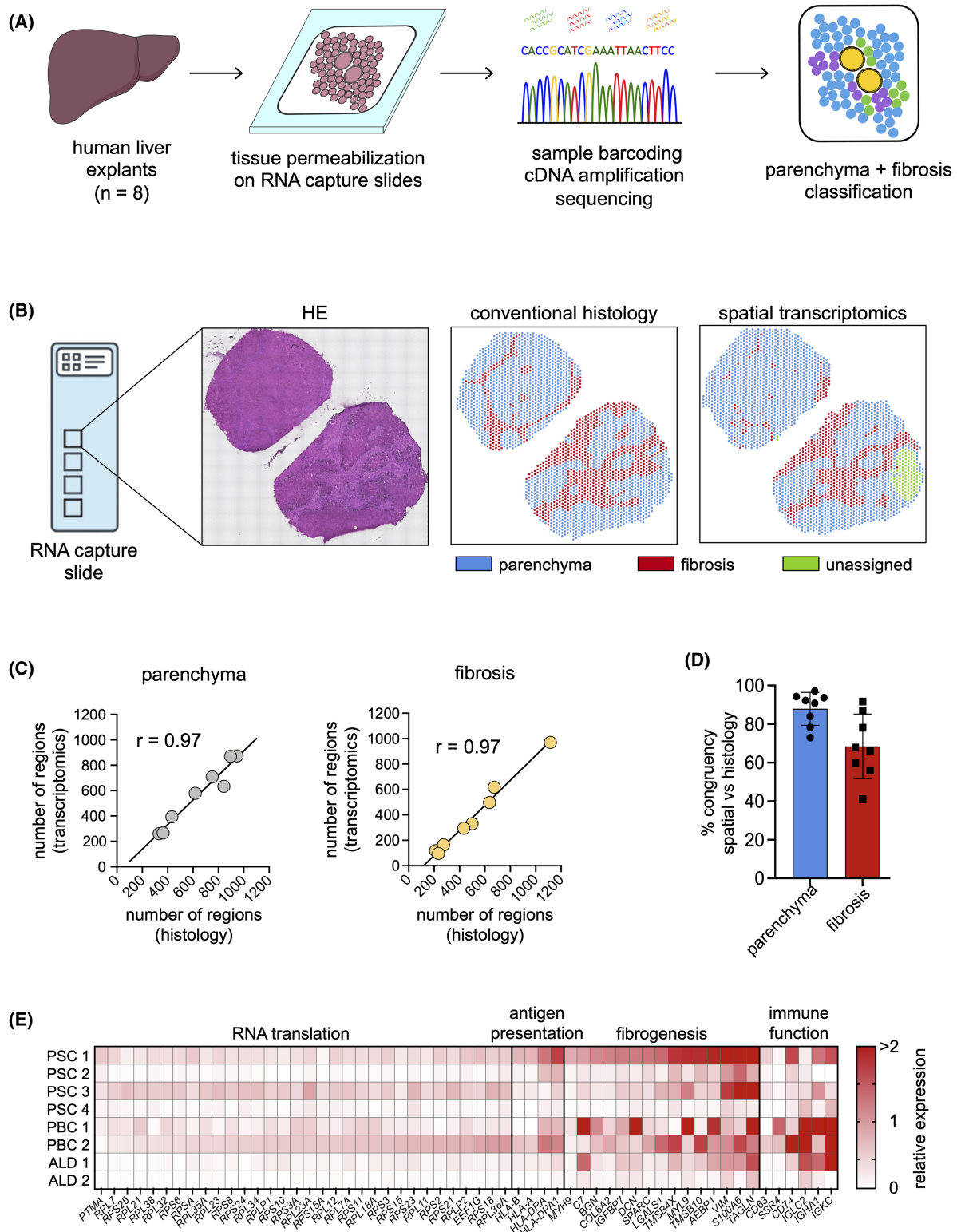
FIGURE 1 Classification of parenchymal and fibrotic regions by spatial transcriptomics. (A) Overview of spatial transcriptomics pipeline. Snap-frozen liver tissue was sectioned, stained, and permeabilized on RNA capture slides. Whole-tissue transcriptomes were tagged with region barcodes, amplified, sequenced, aligned to the human genome (GRCh38), and analyzed by graph-based clustering. (B) Classification of parenchymal and fibrotic liver regions (i.e., RNA capture spots) by conventional histology or spatial transcriptomics. Unassigned regions represent areas of low RNA counts as measured by spatial transcriptomics. Hematoxylin and eosin (HE) staining for assessment by conventional histological shown for reference. (C) Spearman correlation (r) of parenchymal and fibrotic classification using spatial transcriptomics and histology (n = 8 liver samples). (D) Percentage of classification congruency between identical RNA capture spots defined as parenchymal or fibrotic by spatial transcriptomics and histology (n = 8 livers). (E) Differentially expressed gene analysis of parenchymal and fibrotic liver regions for each explant sample. Significantly up-regulated genes are shown ($p < 0.05$) and grouped into biological processes defined by STRING protein–protein pathway analyses.

Spatial transcriptomics identifies localization of cell types enriched in human liver fibrosis

Recent scRNAseq and bulk RNA sequencing studies have shown that specific mesenchymal, endothelial, and monocyte lineages are enriched in cirrhotic livers.[7,8,19] To determine whether these populations and other cell types preferentially reside in fibrotic liver areas, we first used published scRNAseq data of hepatocytes, mesenchyme, endothelia, cholangiocytes, pDCs, mast cells, monocytes, ILCs, B cells, T cells, and cycling cell types found in human cirrhotic explants,[7] and used these data to generate gene profiles for each cell type (i.e., "signature matrices") using the open-access gene deconvolution tool CIBERSORTx[20] (Figure 2A and Table S1; 11 clusters). Signature matrices for the 11 major cell types were then used in CIBERSORTx to deconvolute spatial transcriptomes and estimate the proportion of each cell type in regions defined as parenchymal or fibrotic by spatial transcriptomics.

By combining scRNAseq, spatial transcriptomics and gene deconvolution, we detected a significant enrichment of estimated hepatocytes, cholangiocytes, and cycling cells (consisting of proliferating ILCs, monocytes and T cells) in parenchymal regions and mesenchymal, endothelial, monocyte, ILC, B cell, and T cell lineages in fibrotic areas (Figure 2B). In particular, hepatocytes in liver parenchyma and total mesenchymal cells, monocytes, T cells, and B cells in areas of liver fibrosis were significantly enriched and detected at 2.5-fold greater frequencies compared with their respective fibrotic or parenchymal counterparts. Estimated frequencies of endothelial subsets were also significant enriched in fibrotic areas versus parenchymal regions (1.9-fold) by CIBERSORTx analysis and quantitatively substantiated at the protein level by CD31 immunofluorescence staining of liver sections cut from the same tissue blocks used for spatial transcriptomics (Figure S4). Minor differences were observed in the frequencies of mesenchymal cells and monocytes in fibrotic areas of different liver etiologies (Figure S5); however, most cell types were observed at similar frequencies across livers and consistent with a diagnosis of end-stage cirrhosis for all patients (Table 1). Localization of cell types using selected lineage markers (Table 2) to regions defined as parenchymal or fibrotic by spatial transcriptomics confirmed that hepatocytes (*NNMT+* and *APOC1+*) reside at higher proportions in liver parenchyma on average (2.9-fold, $p < 0.0001$), compared with areas of fibrosis, whereas mesenchymal cells (2.4-fold, $p = 0.008$), monocytes (1.6-fold, $p = 0.0028$), T cells (1.5-fold, $p = 0.0059$), and B cells (1.5-fold, $p = 0.04$) were enriched in fibrotic regions compared with liver parenchyma (Figure 2C,D and Figure S6). Immunofluorescence staining of liver sections from the same tissue blocks used for spatial transcriptomics showed strong protein expression of NNMT on hepatocytes in parenchymal regions

and COL3A1, C1QC, CD3D, and IGHM corresponding to mesenchyme, monocytes, T cells and B cells in fibrotic regions (Figure 2E). Immune cell types defined as enriched in parenchymal areas by CIBERSORTx analysis of spatial transcriptomes appeared largely uniform in distribution throughout the periportal (*ALB* and phosphoenolpyruvate carboxykinase 1 [*PCK1*]), midzonal (cytochrome P450 family 2 subfamily E member 1 [*CYP2E1*]), and midzonal-central (*CYP1A2*, apolipoprotein E [*APOE*], and glutamate-ammonia ligase [*GLUL*]) liver zonation regions (Figure S7).[21]

Mesenchymal cell states localize to fibrotic liver septa

To further pinpoint the spatial distribution of cell types in liver fibrosis, we stratified the 11 major liver lineages into 44 cell states (Table S1; 44 clusters) as previously defined by scRNAseq of cirrhotic livers.[7] As mesenchyme was estimated as the largest cell fraction in fibrotic regions (Figure 2A), we first subdivided the main mesenchymal compartment into four cell states consisting of vascular smooth muscle cells (VSMC), hepatic stellate cells (HSC), scar-associated mesenchymal cells (SAMes), and mesothelia (Figure 3A). CIBERSORTx gene deconvolution of spatial transcriptomes from parenchymal and fibrotic regions revealed significant enrichments of HSC and SAMes in regions of fibrosis, while VSMC were rare and present at far greater estimated proportions in parenchymal areas (Figure 3B). Localized enrichment of HSC and SAMes to fibrotic areas classified by spatial transcriptomics mapped back to digitized tissue images using the marker genes *ACTA2* and *FAPB4* for HSC and *COL3A1* for SAMes (Figure 3C and Figure S8). Coexpression of ACTA2 and FAPB4 was also detected by immunofluorescence staining of liver sections cut from the same tissue blocks used for spatial transcriptomics (Figure 3D). No significant differences in the frequencies of mesenchymal cell states were noted between livers of different etiologies (Figure S9).

Distinct monocytic states localize to regions of liver fibrosis

To assess whether hematopoietic myeloid cell types are enriched in fibrotic compartments of cirrhotic livers, we again applied CIBERSORTx deconvolution analysis of total gene content measured by spatial transcriptomics (Table S2) and delineated the monocyte population into nine discrete cell states of tissue monocytes (TM-1, TM-2, TM-3), scar-associated macrophage (SAMac-1, SAMac-2), Kupffer cells (KC-1, KC-2), and classical dendritic cells cDC1 and cDC2 (Figure 4A).[7] Estimated frequencies of TM-1, TM-3, and KC-1 were significantly
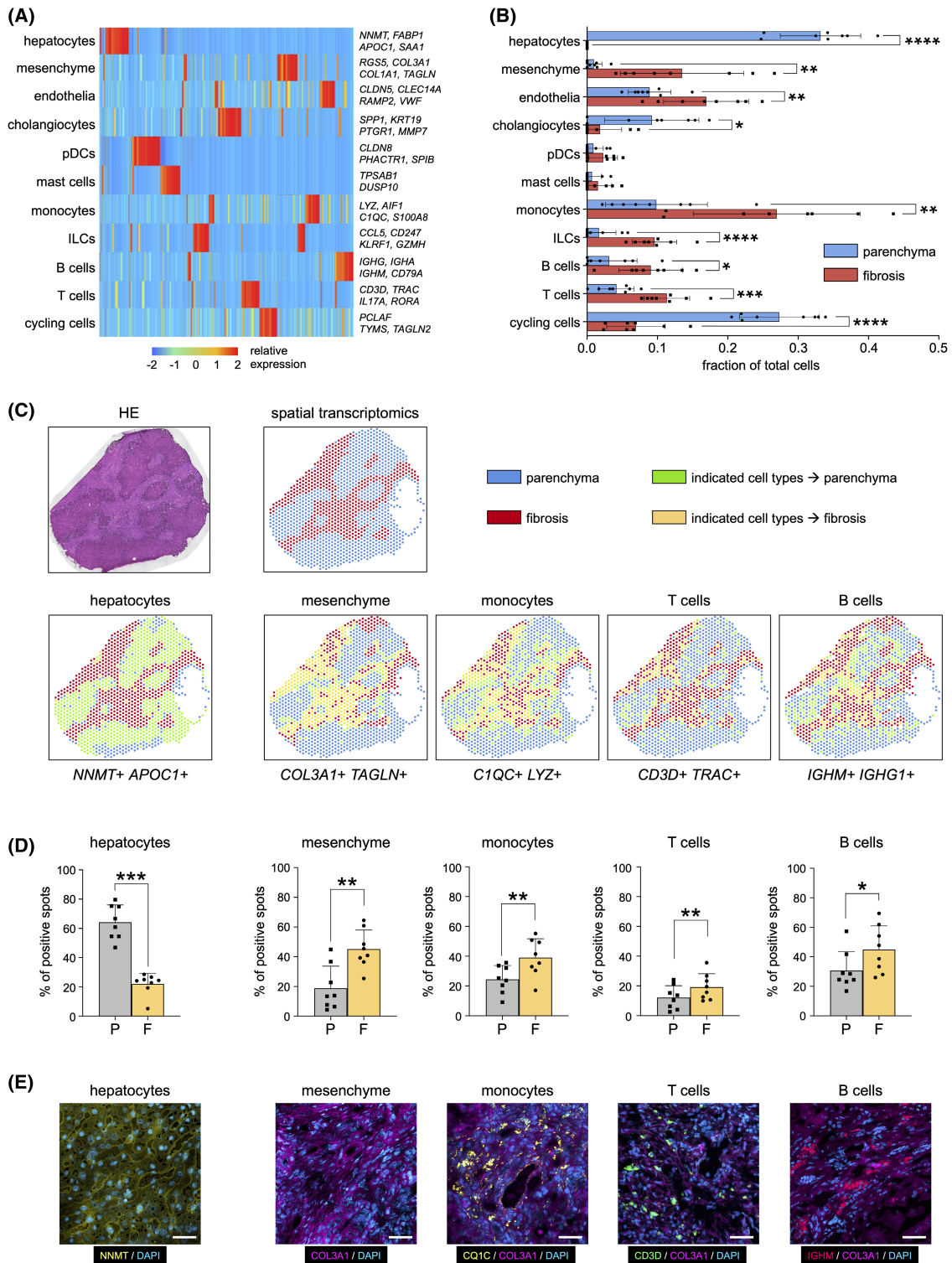
FIGURE 2 Spatial transcriptomics reveals enriched cell types in liver fibrosis. (A) Transcriptional profiles of 11 major liver cell types generated by CIBERSORTx analysis of single-cell RNA sequencing (scRNAseq; n = 10,000 cells). Rows denote cell types; columns denote genes; exemplar lineage markers shown. (B) Fractions of cell types in parenchymal and fibrotic regions as calculated by CIBERSORTx analysis of spatial transcriptomes. (C) Location of cell types detected at 2.5-fold or greater frequencies by CIBERSORTx gene deconvolution of spatial transcriptomes. Hematoxylin and eosin (HE) staining is shown as comparison reference for parenchymal (blue) and fibrotic (red) liver regions classified by spatial transcriptomics (top row). Indicated cell types detected in parenchyma using shown marker genes appear green, and cell types detected in fibrotic regions appear yellow (bottom row). Absence of indicated cell types in parenchyma appear blue; fibrosis regions without indicated cell types appear red. (D) Percentages of each indicated cell type using shown marker genes in parenchymal (P) and fibrotic (F) regions of cirrhotic human liver samples. (E) Immunofluorescence staining of liver sections from the same tissue blocks used for spatial transcriptomics. Hepatocytes are marked by nicotinamide N-methyltransferase (NNMT; yellow), mesenchyme by collagen type III alpha 1 chain (COL3A1; magenta), monocytes by complement C1q C chain (C1QC; yellow), T cells by CD3D (green), and B cells by immunoglobulin heavy constant mu (IGHM; red). Nuclei stained by DAPI (blue). Scale bars, 50 μm. *$p < 0.05$, **$p < 0.01$, ***$p < 0.001$, ****$p < 0.0001$.

enriched in fibrotic regions, whereas gene signatures corresponding to TM-2, KC-2, and cDC1 monocyte states were increased in parenchyma (Figure 4B). Enrichment of TM-1, TM-3, and KC-1 to fibrotic areas as defined by spatial transcriptomics was mapped to digitized tissue images using the marker genes *IL17RA*+ and *S100A8*+

TABLE 2 Marker genes for the supervised identification of cell types in RNA capture spots detected at 2.5-fold higher frequencies in parenchymal or fibrotic liver regions by CIBERSORTx analysis

Cell type	Marker genes
hepatocytes	*NNMT, APOC1*
mesenchyme	*COL3A1, TAGLN*
monocytes	*C1QC, LYZ*
T cells	*CD3D, TRAC*
B cells	*IGHM, IGHG1*

Abbreviations: *APOC1*, apolipoprotein C1; *C1QC*, complement C1q C chain; *COL3A1*, collagen type III alpha 1 chain; *IGHM*, immunoglobulin heavy constant mu; *IGHG1*, immunoglobulin heavy constant gamma 1; *LYZ*, lysozyme; *NNMT*, nicotinamide N-methyltransferase; *TAGLN*, transgelin; *TRAC*, T cell receptor alpha constant.

for TM-1, *FCER1G1*+ for TM-3, and *VCAM1*+ and *SDC3*+ for KC-1 monocyte subtypes (Figure 4C and Figure S10). Immunofluorescence staining of liver sections from the same tissue blocks used for spatial transcriptomics showed strong co-expression of VCAM1 on CD68+ monocytes (Figure 4D). No significant differences in the frequencies of monocyte states were noted between livers of different etiologies (Figure S11).

Increased proportion of T cell and B cell subtypes in liver fibrosis

As lymphocytes constitute a significant proportion of liver infiltration in cirrhotic liver,[22] we lastly applied CIBERSORTx deconvolution analysis to gene content of parenchymal and fibrotic liver areas (Table S2) and estimated the proportion of distinct T cell and B cell states previously defined by scRNAseq.[7] Bulk T cells were subdivided into five cell states (T cells-1 to T cells-5), and the major B cell compartment was
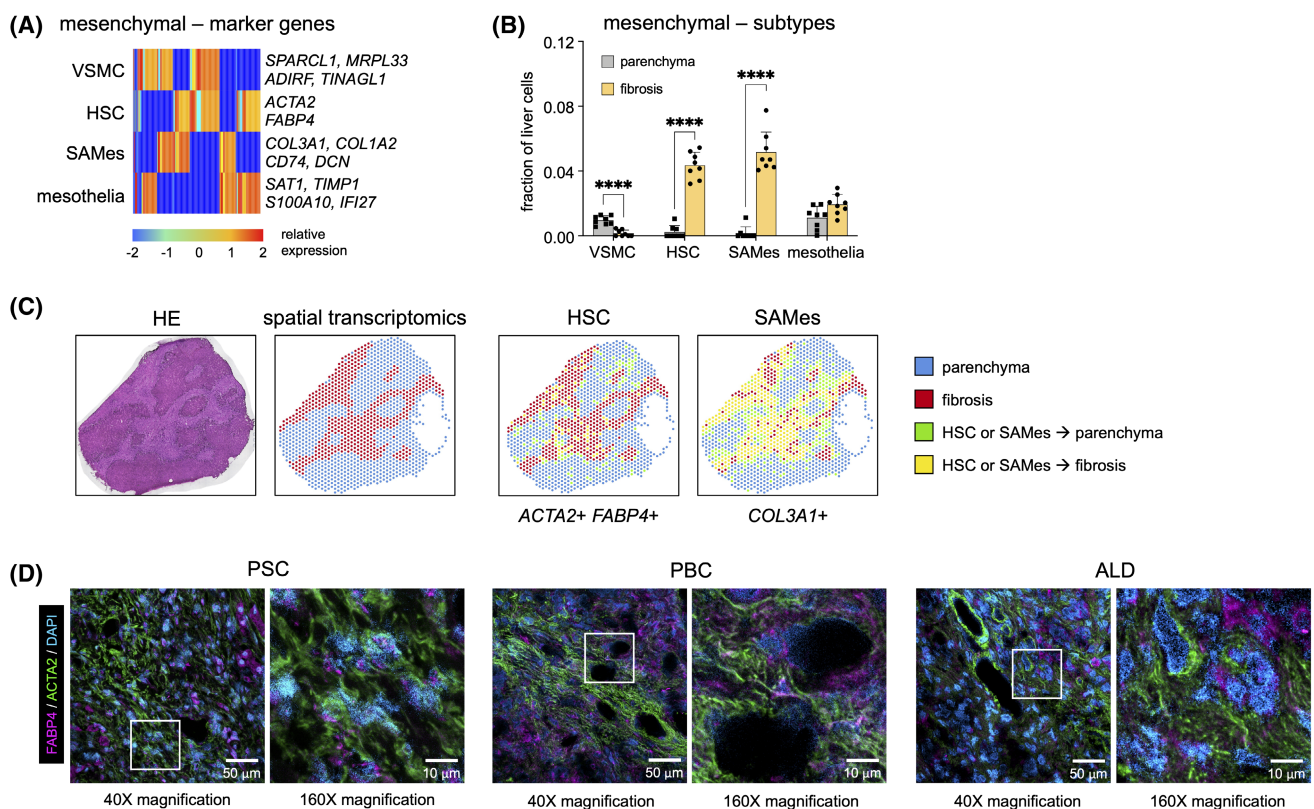
FIGURE 3 Mesenchymal cell states localize to fibrotic liver septa. (A) Transcriptional profiles of mesenchymal cell types generated by CIBERSORTx analysis of scRNAseq. Rows denote cell types; columns denote genes; exemplar lineage markers are shown. (B) Fractions of mesenchymal lineages in parenchymal and fibrotic regions as calculated by CIBERSORTx analysis of spatial transcriptomes (*n* = 8 livers). (C) Hematoxylin and eosin (HE) staining shown as comparison reference for parenchymal (blue) and fibrotic (red) liver regions classified by spatial transcriptomics (left). Detection of hepatic stellate cells (HSC) and scar-associated mesenchymal cell (SAMes) subtypes in parenchyma using shown marker genes appear green, and in fibrotic regions appear yellow (right). Parenchyma without HSC or SAMes cell types appear blue; fibrotic regions without HSC or SAMes appear red. (D) Immunofluorescence staining of primary sclerosing cholangitis (PSC), primary biliary cholangitis (PBC), and alcohol-related liver disease (ALD) liver sections show expression of fatty acid–binding protein 4 (FABP4; magenta) on HSC (actin alpha 2, smooth muscle [ACTA2]; green). Nuclei stained by 4′,6-diamidino-2-phenylindole (DAPI; blue). ****$p < 0.0001$.

recategorized into four cell states (B cells-1, B cells-2, plasma cells-1, and plasma cells-2) (Figure 5A,D). Estimated frequencies T cells-3, T cells-4, and T cells-5 were significantly enriched in fibrotic septae, while gene signatures corresponding to the T cells-1 subset were increased in parenchyma (Figure 5B). In contrast, estimated frequencies of all B cell states were elevated in liver fibrosis, with B cells-1, B cells-2, and plasma cells-2 estimated to be significantly enriched (Figure 5E). Localization of T cells-3, T cells-4, and T cells-5 to areas defined as fibrotic by spatial transcriptomics was mapped to digitized tissue images using the selected gene markers chemokine (C-C motif) ligand 4 (*CCL4*), *CCL5*, and killer cell lectin like receptor B1 (*KLRB1*) for T cells-3 and T cells-4, and granzyme A (*GZMA*) and *CD53* for T cells-5 (Figure 5C and Figure S12). Localized enrichment of B cells-1 and B cells-2 and plasma cells-2 to fibrotic areas using spatial transcriptomics was mapped to digitized tissue images using the marker genes major histocompatbility complex, class II, DR (*HLA-DR*), *CD37*, and C-X-C motif chemokine receptor 4 (*CXCR4*) for B cells-1 and B cells-2, and *IGHM* and immunoglobulin heavy chain gamma (*IGHG*) for plasma cells-2 (Figure 5F and Figure S12). In contrast to T cell subtypes, estimated frequencies of B cell states in livers of different etiologies were markedly distinct, as greater proportions of plasma cells-2 were detected in regions of PBC fibrosis as defined by spatial transcriptomics compared with PSC (4.1-fold lower, $p < 0.05$) and ALD samples (6.2-fold lower, $p < 0.05$; Figure S13).

DISCUSSION

This study uses whole-tissue spatial transcriptomics to determine the localization of gene content and cell types enriched in human liver fibrosis. We demonstrate that gene expression directly measured by spatial transcriptomics from different areas of cirrhotic livers is distinct and strongly correlates with conventional classification of parenchymal and fibrotic liver regions by histopathology, regardless of disease etiology. We also show the power of applying spatial transcriptomics to define gene content of specific liver regions first and then exploiting high-resolution scRNAseq and gene deconvolution to estimate the fraction of localized cell types. Using this combinatorial approach, we detected significantly increased fractions of endothelial, ILCs, and cycling cells in fibrotic areas defined by spatial transcriptome analysis. Moreover, estimated total frequencies of mesenchymal, monocyte, B cell, and T cell lineages within fibrotic regions were estimated at greater than 2.5-fold higher compared with parenchyma, suggesting that these subsets may be key players limiting or exacerbating liver fibrosis during the progression of cirrhosis. Together, these findings support that gene content

within areas of fibrosis reflects the presence of specific cell types, and these distinct cell states may regulate important pathogenic pathways involved in chronic fibrogenesis. The use of spatial transcriptomics and total gene content also represents an important proof of concept and advance over traditional transcriptome technologies like RNA sequencing, single-molecule fluorescence *in situ* hybridization, or scRNAseq, which are either biased *a priori* by the availability and preselection of specific probes or limited by sufficient sample material and necessity of cell suspensions that destroy the tissue architecture, which minimize the detailed assessment of localized cellular interactions.

In line with scRNAseq of cirrhotic explants,[7] our assessment of liver cell subsets by spatial transcriptomics and CIBERSORTx analysis uncovered significantly increased frequencies of *ACTA2+ FABP4+* and *COL3A1+* mesenchymal cells (HSC and SAMes) in fibrotic compartments of end-stage livers. These results are comparable to murine models of liver fibrosis, which show mesenchymal cell types analogous to human HSC and SAMes increased during fibrogenesis,[23] and RNA velocity analysis of cirrhotic human livers, which have established a clear convergence of VSMC and HSC toward SAMes states during fibrogenesis.[7,24] Our spatial transcriptome analysis also revealed significantly greater proportions of lymphocyte subsets in areas of liver fibrosis, particularly *CCL4+ CCL5+ KLRB1+* and *GZMA+ IL17RA+* T cell states (T cells-3, T cells-4, and T cells-5), *HLA-DR+ CD37+ CXCR4+* B cells (B cells-1 and B cells-2), and *IGHM+ IGHG+* plasma cells (plasma cells-2). These observations are consistent with previous findings that large producers of CCL4 and CCL5, including innate-like gamma-delta T cells, invariant natural killer T cells, and regulatory T cells, are increased in diseased livers,[25–27] as are infiltrating B cell/plasma cell lineages that produce autoantibodies.[22] Although appealing, it is speculative to assign a precise pathogenic or protective role in fibrogenesis for any of these enriched cell states given the limited number of analyzed samples herein. It should be emphasized that several of these markers have been reported on other cell types (e.g., *FABP4* on endothelial cells, *VCAM1* on endothelial cells) and should therefore be assessed in concert with additional markers to maximize cellular resolution.[28,29]

While most of our results align with previous findings, we also observed conflicting indications of enriched cell states using spatial transcriptomics and gene deconvolution. One example was the estimated proportion of KC-1 monocyte subtypes in fibrosis, in which our findings indicated KC-1 was significantly increased whereas scRNAseq analysis found KC-1 was significantly decreased in cirrhotic livers compared with healthy samples.[7] These differences likely illustrate our comparison of parenchymal and fibrotic regions within the same cirrhotic liver samples instead
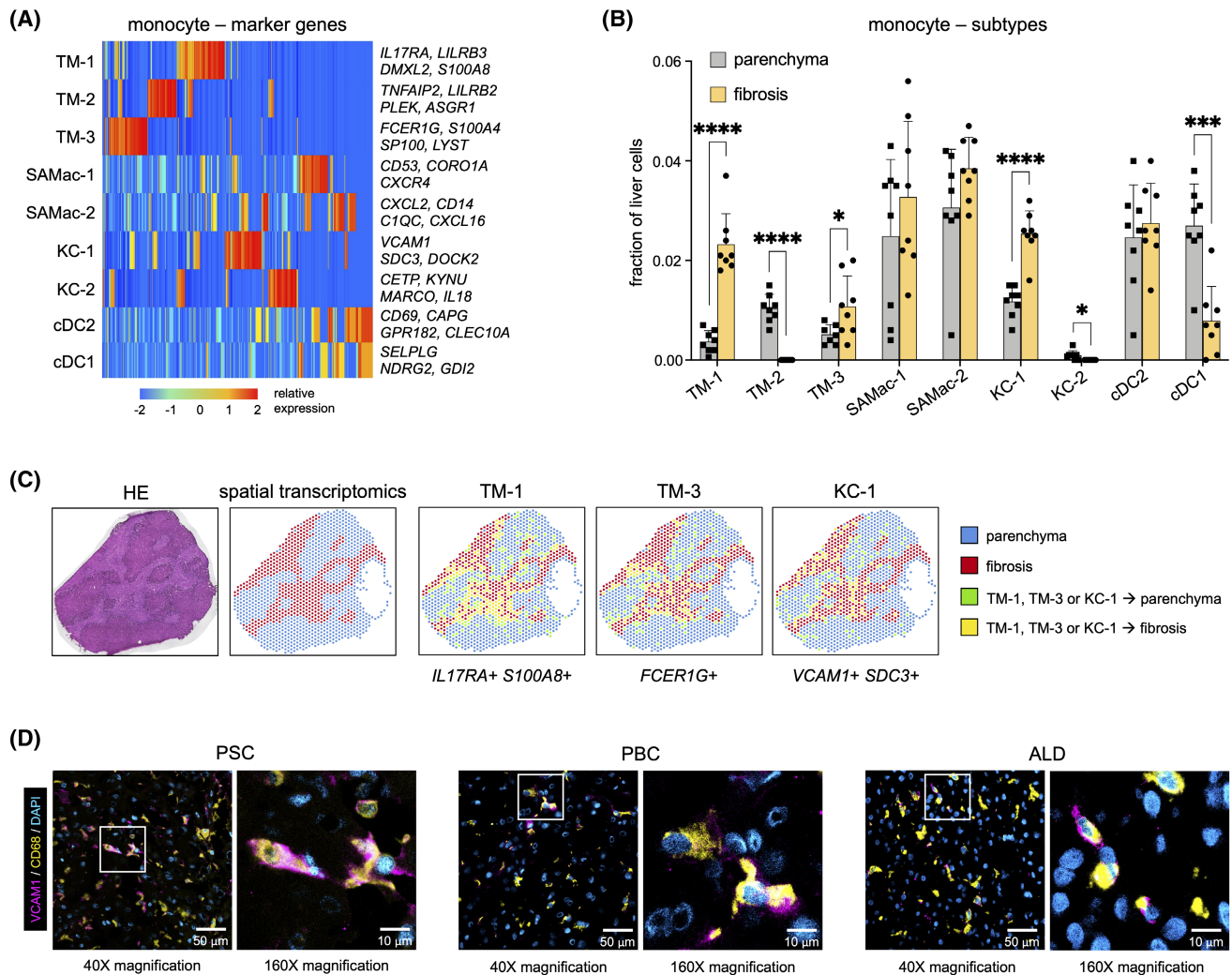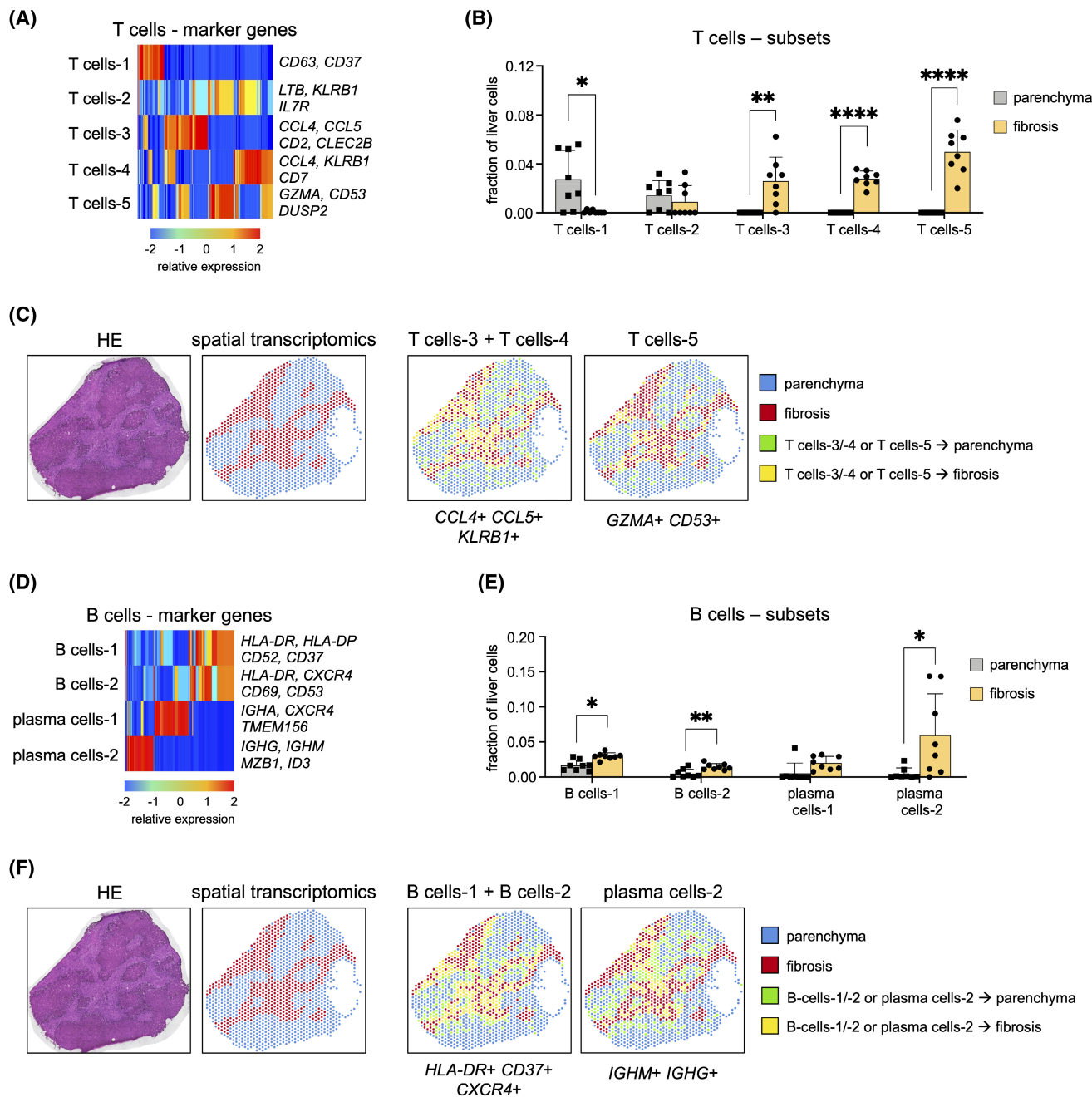
FIGURE 4 Distinct monocyte states localize to regions of liver fibrosis. (A) Transcriptional profiles of monocytes generated by CIBERSORTx analysis of scRNAseq. Rows denote cell types; columns denote genes; exemplar lineage markers are shown. (B) Fractions of monocyte states in parenchymal and fibrotic regions calculated by CIBERSORTx analysis of spatial transcriptomes ($n = 8$ livers). (C) Hematoxylin and eosin (HE) staining shown as comparison reference for parenchymal (blue) and fibrotic (red) liver regions classified by spatial transcriptomics (left). Detection of TM-1, TM-3, and KC-1 mesenchymal subtypes in parenchyma using shown marker genes appear green and in fibrotic regions appear yellow (right). Parenchyma without TM-1, TM-3, and KC-1 cell types appear blue; fibrotic regions without TM-1, TM-3, and KC-1 appear red. (D) Immunofluorescence staining of PSC, PBC, and ALD liver sections shows co-expression of vascular cell adhesion molecule 1 (VCAM1; magenta) on CD68+ monocytes (yellow). Nuclei stained by DAPI (blue). *$p < 0.05$, ***$p < 0.001$, ****$p < 0.0001$.

of comparisons to healthy control livers and may relate to differences in the migration and expansion of specific cell populations between individual patients and/or disease etiologies, showing that larger studies using these methodologies are necessary to unpick patient-intrinsic and disease-intrinsic cell networks. Our discrepant findings regarding KC-1 may also reflect analytical errors associated with the generation and use of distinct gene profiles for CIBERSORTx enumeration, as an unexpected proportion of lineage marker genes identified by scRNAseq used to separate closely related cell types were absent or detected at very low levels by spatial transcriptomics.[7] Ongoing development of spatial technology will undoubtedly yield greater granularity, and complementary methods such

as multi-dimensional immunohistochemistry together with spatial transcriptomics should aid the overall resolution of cellular phenotyping and mitigate ambiguous cell assignments in future studies.[13,30]

In addition to discrepant cell frequencies, we unexpectedly detected cell-specific gene expression in tissue regions containing few of these cell types, as determined by traditional histology. This phenomenon was most evident when analyzing hepatocyte gene expression, as we detected relatively high levels of albumin and other hepatocyte-specific RNA content in fibrotic regions. This may partly be explained by the presence of hepatocytes, individually or in small clusters, which were difficult to identify in the fibrotic areas due to resolution limitations of the histological images.

FIGURE 5 Subsets of T cells and B cells are enriched in regions of liver fibrosis. Transcriptional profiles of T cells (A) and B cells (D) generated by CIBERSORTx analysis of scRNAseq. Rows denote cell types; columns denote genes; exemplar lineage markers are shown. Fractions of T cell (B) and B cell states (E) in parenchymal and fibrotic regions calculated by CIBERSORTx analysis of spatial transcriptomes ($n = 8$ livers). T cells-3, T cells-4, and T cells-5 (C) and B cells-1, B cells-2, and plasma-cells-2 (F) are detected using shown marker genes. Hematoxylin and eosin (HE) staining shown as comparison reference for parenchymal (blue) and fibrotic (red) liver regions classified by spatial transcriptomics (left). Detection of indicated cell subtypes in parenchyma using shown marker genes appear green and in fibrotic regions appear yellow (right). Parenchyma devoid of indicated cell types appear blue; fibrotic regions without indicated cell subtypes appear red. $*p < 0.05$, $**p < 0.01$, $****p < 0.0001$.

However, spillover of localized transcripts into adjacent areas likely also occurred, as we detected RNA content in capture regions outside of the tissue boundaries and these gene signatures closely resembled those of the neighboring tissue (Figure S2). Increased spillover may have resulted from our efforts to maximize RNA release from fibrotic regions, as we suspect that a disproportional release of transcripts from parenchymal regions with high transcriptional activity may be subsequently captured in areas of lower gene expression such as regions of liver fibrosis. The degree of permeabilization should therefore be carefully balanced versus potential

spillover effects, and downstream quality-control and normalization procedures should be applied before final analyses to minimize imprecise localization of gene content. We believe that additional optimization of tissue permeabilization, limiting RNA release while retaining sufficient signal output is achievable, and further improvements in capture density should lessen the degree of off-target findings using spatial transcriptomics technologies.

In summary, we present an application of spatial transcriptomics for the cellular characterization of liver fibrosis in human cirrhotic explants. Our results can serve as a basis for more detailed future studies using liver tissue from earlier stages/time points of disease, to assess the involvement of specific molecules and pathways related to disease stage as well as possible links between the genetic and cellular signatures of liver fibrosis. Despite analytical and methodological limitations, our findings justify combining additional "omics" approaches in future efforts to unravel the regulatory networks involved in liver fibrosis and identify molecular targets that can inform the development of effective antifibrotic therapies.

AUTHOR CONTRIBUTIONS
Study design: Brian K. Chung and Espen Melum. *Histological assessment*: Henrik Mikael Reims and Jonas Øgaard. *Spatial transcriptomics*; Brian K. Chung and Jonas Øgaard. *Data analysis*: Brian K. Chung, Jonas Øgaard, and Henrik Mikael Reims. *Data interpretation*: Brian K. Chung, Jonas Øgaard, Henrik Mikael Reims, and Espen Melum. *Manuscript draft*: Brian K. Chung and Espen Melum. *Clinical samples*: Tom Hemming Karlsen and Espen Melum. All authors revised the manuscript and approved the final version.

ORCID
Brian K. Chung https://orcid.org/0000-0002-9523-7515
Espen Melum https://orcid.org/0000-0001-6903-6878

REFERENCES
1. GBD 2017 Causes of Death Collaborators. Global, regional, and national age-sex-specific mortality for 282 causes of death in 195 countries and territories, 1980–2017: a systematic analysis for the global burden of disease study 2017. Lancet. 2018;392:1736–88.
2. Penz-Österreicher M, Österreicher CH, Trauner M. Fibrosis in autoimmune and cholestatic Liver disease. Best Pract Res Clin Gastroenterol. 2011;25:245–58.
3. Angulo P, Kleiner DE, Dam-Larsen S, Adams LA, Bjornsson ES, Charatcharoenwitthaya P, et al. Liver fibrosis, but no other histologic features, is associated with long-term outcomes of patients with nonalcoholic fatty Liver disease. Gastroenterology. 2015;149:389–97.e10.
4. European Association for the Study of the Liver, Angeli P, Bernardi M, Villanueva C, Francoz C, Mookerjee RP, et al. EASL clinical practice guidelines for the management of patients with decompensated cirrhosis. J Hepatol. 2018;69:406–60.
5. Ramachandran P, Henderson NC. Antifibrotics in chronic liver disease: tractable targets and translational challenges. Lancet Gastroenterology Hepatol. 2016;1:328–40.
6. Chu AL, Schilling JD, King KR, Feldstein AE. The power of single-cell analysis for the study of liver pathobiology. Hepatology. 2021;73(1):437–48.
7. Ramachandran P, Dobie R, Wilson-Kanamori JR, Dora EF, Henderson BEP, Luu NT, et al. Resolving the fibrotic niche of human liver cirrhosis at single-cell level. Nature. 2019;575:512–8.
8. Poch T, Krause J, Casar C, Liwinski T, Glau L, Kaufmann M, et al. Single-cell atlas of hepatic T cells reveals expansion of liver-resident naive-like CD4+ T cells in primary sclerosing cholangitis. J Hepatol. 2021;75:414–23.
9. Stubbington MJT, Rozenblatt-Rosen O, Regev A, Teichmann SA. Single-cell transcriptomics to explore the immune system in health and disease. Science. 2017;358:58–63.
10. Saviano A, Henderson NC, Baumert TF. Single-cell genomics and spatial transcriptomics: discovery of novel cell states and cellular interactions in liver physiology and disease biology. J Hepatol. 2020;73:1219–30.
11. Sharma A, Seow JJW, Dutertre C-A, Pai R, Blériot C, Mishra A, et al. Onco-fetal reprogramming of endothelial cells drives immunosuppressive macrophages in hepatocellular carcinoma. Cell. 2020;183:377–94.e21.
12. Andrews TS, Atif J, Liu JC, Perciani CT, Ma XZ, Thoeni C, et al. Single-cell, single-nucleus, and spatial RNA sequencing of the human liver identifies cholangiocyte and mesenchymal heterogeneity. Hepatology Commun. 2022;6(4):821–40.
13. Guilliams M, Bonnardel J, Haest B, Vanderborght B, Wagner C, Remmerie A, et al. Spatial proteogenomics reveals distinct and evolutionarily conserved hepatic macrophage niches. Cell. 2022;185:379–96.e38.
14. Karlsen TH, Folseraas T, Thorburn D, Vesterhus M. Primary sclerosing cholangitis—a comprehensive review. J Hepatol. 2017;67:1298–323.

15. Gulamhusein AF, Hirschfield GM. Primary biliary cholangitis: pathogenesis and therapeutic opportunities. Nat Rev Gastroentero. 2019;17:93–110.
16. Gao B, Bataller R. Alcoholic liver disease: pathogenesis and new therapeutic targets. Gastroenterology. 2011;141: 1572–85.
17. Bankhead P, Loughrey MB, Fernández JA, Dombrowski Y, McArt DG, Dunne PD, et al. QuPath: open source software for digital pathology image analysis. Sci Rep. 2017;7:16878.
18. Szklarczyk D, Gable AL, Nastou KC, Lyon D, Kirsch R, Pyysalo S, et al. The STRING database in 2021: customizable protein–protein networks, and functional characterization of user-uploaded gene/measurement sets. Nucleic Acids Res. 2021;49:D605–12.
19. Kim A, Wu X, Allende DS, Nagy LE. Gene deconvolution reveals aberrant liver regeneration and immune cell infiltration in alcohol-associated hepatitis. Hepatology. 2021;74:987–1002.
20. Newman AM, Steen CB, Liu CL, Gentles AJ, Chaudhuri AA, Scherer F, et al. Determining cell type abundance and expression from bulk tissues with digital cytometry. Nat Biotechnol. 2019;37:773–82.
21. Aizarani N, Sagar AS, Mailly L, Durand S, Herman JS, Pessaux P, et al. A human liver cell atlas reveals heterogeneity and epithelial progenitors. Nature. 2019;572:199–204.
22. Chung BK, Guevel BT, Reynolds GM, Udatha DBRKG, Henriksen EKK, Stamataki Z, et al. Phenotyping and auto-antibody production by liver-infiltrating B cells in primary sclerosing cholangitis and primary biliary cholangitis. J Autoimmun. 2017;77:45–54.
23. Iwaisako K, Jiang C, Zhang M, Cong M, Moore-Morris TJ, Park TJ, et al. Origin of myofibroblasts in the fibrotic liver in mice. Proc National Acad Sci. 2014;111:E3297–305.
24. Wang Z-Y, Keogh A, Waldt A, Cuttat R, Neri M, Zhu S, et al. Single-cell and bulk transcriptomics of the liver reveals potential targets of NASH with fibrosis. Sci Rep. 2021;11:19396.
25. Chen Y, Jeffery HC, Hunter S, Bhogal R, Birtwistle J, Braitch MK, et al. Human intrahepatic regulatory T cells are functional, require IL-2 from effector cells for survival, and are susceptible to Fas ligand-mediated apoptosis. Hepatology. 2016;64:138–50.
26. Berres M-L, Koenen RR, Rueland A, Zaldivar MM, Heinrichs D, Sahin H, et al. Antagonism of the chemokine Ccl5 ameliorates experimental liver fibrosis in mice. J Clin Invest. 2010;120:4129–40.
27. Hunter S, Willcox CR, Davey MS, Kasatskaya SA, Jeffery HC, Chudakov DM, et al. Human liver infiltrating γδ T cells are composed of clonally expanded circulating and tissue-resident populations. J Hepatol. 2018;69:654–65.
28. Halpern KB, Shenhav R, Massalha H, Toth B, Egozi A, Massasa EE, et al. Paired-cell sequencing enables spatial gene expression mapping of liver endothelial cells. Nat Biotechnol. 2018;36:962–70.
29. Furuta K, Guo Q, Pavelko KD, Lee J-H, Robertson KD, Nakao Y, et al. Lipid-induced endothelial vascular cell adhesion molecule 1 promotes nonalcoholic steatohepatitis pathogenesis. J Clin Invest. 2021;131:e143690.
30. Chen Y, Shen Q, White SL, Gokmen-Polar Y, Badve S, Goodman LJ. Three-dimensional imaging and quantitative analysis in CLARITY processed breast cancer tissues. Sci Rep. 2019;9:5624–13.

SUPPORTING INFORMATION

Additional supporting information may be found in the online version of the article at the publisher's website.

How to cite this article: Chung BK, Øgaard J, Reims HM, Karlsen TH, Melum E. Spatial transcriptomics identifies enriched gene expression and cell types in human liver fibrosis. Hepatol Commun. 2022;6:2538–2550. https://doi.org/10.1002/hep4.2001